IOP Publishing Nanotechnology
Nanotechnology **25** (2014) 295201 (8pp) doi:10.1088/0957-4484/25/29/295201

Tunable double and triple quantum dots in carbon nanotube with local side gates

Bum-Kyu Kim[1,2], Minky Seo[3,4], Sung Un Cho[2,4], Yunchul Chung[3], Nam Kim[2], Myung-Ho Bae[2] and Ju-Jin Kim[1]

[1] Department of Physics, Chonbuk National University, Jeonju 561-756, Republic of Korea
[2] Korea Research Institute of Standards and Science, Daejeon 305-340, Republic of Korea
[3] Department of Physics, Pusan National University, Busan 609-735, Republic of Korea

E-mail: mhbae@kriss.re.kr and jujinkim@chonbuk.ac.kr

Received 4 April 2014, revised 9 May 2014
Accepted for publication 21 May 2014
Published 1 July 2014

Abstract

We demonstrate a simple but efficient design for forming tunable single, double and triple quantum dots (QDs) in a sub-μm-long carbon nanotube (CNT) with two major features that distinguish this design from that of traditional CNT QDs: the use of i) Al_2O_x tunnelling barriers between the CNT and metal contacts and ii) local side gates for controlling both the height of the potential barrier and the electron-confining potential profile to define multiple QDs. In a serial triple QD, in particular, we find that a stable molecular coupling state exists between two distant outer QDs. This state manifests in anti-crossing charging lines that correspond to electron and hole triple points for the outer QDs. The observed results are also reproduced in calculations based on a capacitive interaction model with reasonable configurations of electrons in the QDs. Our design using artificial tunnel contacts and local side gates provides a simple means of creating multiple QDs in CNTs for future quantum-engineering applications.

Keywords: carbon nanotubes, triple quantum dot, distant coupling

(Some figures may appear in colour only in the online journal)

1. Introduction

Zero-dimensional mesoscopic systems, or so-called 'quantum dots' (QDs), have been identified in various nanostructures, such as single-molecule islands [1], quasi-one-dimensional carbon nanotubes (CNTs) [2], semiconducting nanowires [3] and two-dimensional electron gas (2DEG) GaAs/AlGaAs heterostructures [4]. In particular, single QDs in CNTs have provided a platform for the study of various fundamental phenomena such as Kondo [5], Fano [6] and Fabry–Pérot [7] resonances, including Kondo-superconductivity interactions [8], depending on the coupling strength of the CNTs to the electrical leads. Molecular coupling states in double-QD systems in gate-defined CNTs [9] have also been investigated for their potential application as qubits for future quantum computations [10]. A linear, tunable, triple-QD system has also been identified in a single-walled CNT defined by three top gates [11], where molecular coupling states were observed only between neighbouring QDs. The authors of that study predicted that sufficiently strong coupling strengths between QDs could lead to a distant molecular coupling state between the two outer QDs through a second-order co-tunnelling process. Recently, in a 2DEG-based linear triple-QD system, a direct long-distance coherent molecular coupling between two outer QDs has been observed [12, 13], which suggests a potential method of constructing quantum gates for the single-step control of distant qubits.

To implement such controllable QD systems, the tunnelling barriers between QDs should be precisely tuned to control the interactions between electrons in neighbouring QDs. Generally, the naturally forming Schottky barriers between the semiconducting CNTs and the metal leads have been used as tunnelling barriers [14]. The height of a Schottky barrier, however, is sensitive to the electric fields induced by gates near the contacts, resulting in an uncontrollable change in the charge-carrier tunnelling rates. Multiple top gates [2] and embedded bottom gates [10, 15] have been implemented

[4] Present address: Department of Physics and Astronomy, Seoul National University, Seoul, 151-747, Korea

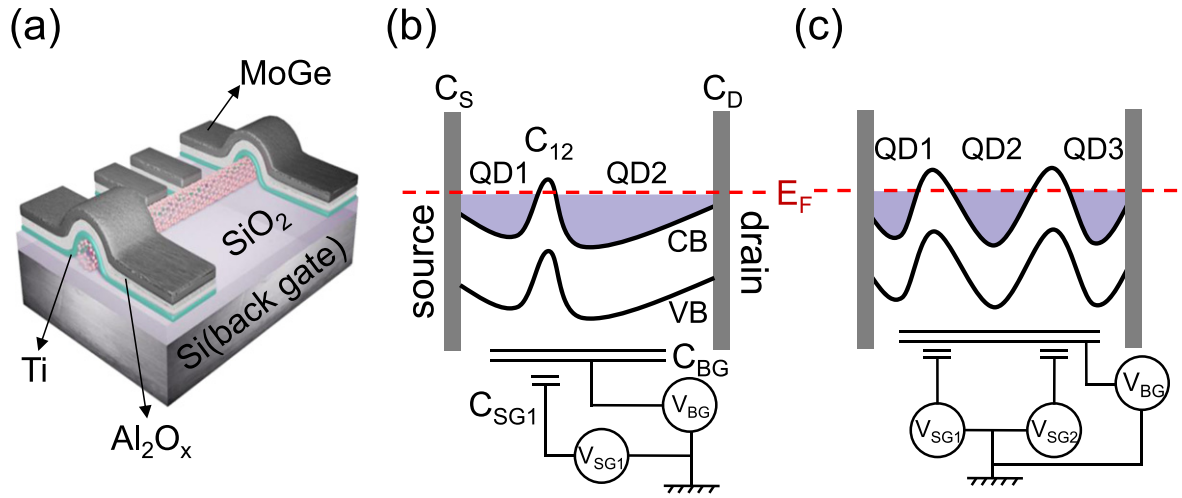

Figure 1. (a) Schematic diagram of the CNT device, in which Al_2O_x layers are served as rigid tunnelling barriers between the metal contacts and the CNT. (b) Schematic diagram illustrating double QD (QD1 and QD2) formation along the CNT with a single side gate (SG1) and a global back gate, where the height of the tunnelling barrier should be higher than the Fermi level in the leads. CB and VB indicate the conduction and valence bands in the CNT, respectively. C_S and C_D represent the source and drain capacitances. C_{SG1}, C_{BG} and C_{12} are the capacitances of the side and back gates, and the coupling capacitance between QD1 and QD2, respectively. (c) Schematic diagram illustrating triple QD (QD1, QD2 and QD3) formation with two side gates (SG1 and SG2) and a global back gate.

to achieve independent control of the energy levels and the contact tunnelling rates. However, in the multiple top gates case, certain defects or additional doping effects may be introduced into the CNT during the gate-insulator deposition process [16, 17], while in the embedded-gate case, positioning the CNT on the gate lines is a challenge.

In this paper, we adopt two strategies to overcome the issues described above: the use of i) Al_2O_x tunnelling barriers between the CNT and the leads and ii) local side gates that form multiple QDs. When a back-gate voltage is applied, the Al_2O_x layers located between the leads and the CNT provide stable tunnelling barriers to form a global potential well along the entire CNT channel. Local side gates near the CNT channel create local potential barriers along the channel, which form multiple potential wells between the two Al_2O_x tunnelling barriers. By varying the applied voltages at the back and local side gates, we demonstrate tunable single, double and triple QDs, as indicated by their corresponding charge-stability diagrams. For the first time, we experimentally produce a distant molecular coupling state between two outer QDs in a linear triple-QD system in a one-dimensional-like CNT. Our calculation results, which are based on a capacitive interaction model, support the existence of distant molecular coupling among the electron configurations in each QD, including the possibility of the existence of a hole quadruple point in our triple QD. The distant coupling in a CNT-QD array should be further examined for future quantum-engineering applications involving charge- or phase-sensitive measurements.

2. Fabrication and experiments

CNTs were grown via chemical vapour deposition in a mixture of argon, hydrogen and methane at ~950 °C from Fe catalysts on a 600 nm-thick SiO_2/Si substrate. A particular CNT can be located by means of pre-patterned alignment markers using atomic force microscopy (AFM) images. After e-beam patterning to fabricate the source, drain and local side gates on a PMMA bi-layer, a Ti (5 nm)/Al (5 nm) bilayer was deposited using an e-beam deposition process at $\sim 3 \times 10^{-7}$ Torr. The thin Al layer was oxidised at ambient pressure. Such an oxidised Al layer has been previously adopted as a robust tunnelling barrier for a CNT device [18]. For the top metal leads, an 80 nm-thick layer of MoGe alloy was sputtered onto the Al_2O_x layer (see figure 1(a)). Highly *p*-doped Si serves as the back-gate electrode. Figures 2(a) and (b) present AFM images of two prepared samples, S1 (channel length $L = 680$ nm and diameter $D \sim 2$ nm) and S2 ($L = 860$ nm and $D \sim 1$ nm). For S1, the distances between the local side gates and the CNT are 130 nm and 190 nm for SG1 and SG2, respectively. For S2, the distance is 130 nm for SG1. All measurements were performed using a two-terminal dc measurement configuration at $T = 4.2$ K.

The schematic diagrams in figures 1(b) and (c) illustrate the formation of double and triple QDs by means of two independent local side gates, SG1 and SG2, and a back gate along a semiconducting (*n*-type) CNT. After a global potential well is prepared between the Al_2O_x tunnelling barriers by applying a positive V_{BG} and, if SG1 is turned on by applying a negative side-gate voltage V_{SG1}, a tunable tunnelling barrier forms in the CNT, as illustrated in figure 1(b), resulting in the formation of double QDs (QD1 and QD2). Here, the height of the inter-dot tunnelling barrier should at least be higher than the Fermi levels in the leads (see figure 1(b)). Furthermore, if both local side gates, SG1 and SG2, are turned on, triple QDs (QD1, QD2 and QD3) form, as illustrated in figure 1(c). Previously, local side gates have been only used to control the energy levels in CNT QDs with a top-gated design [19–21]. Our innovation is to use such local side gates to form

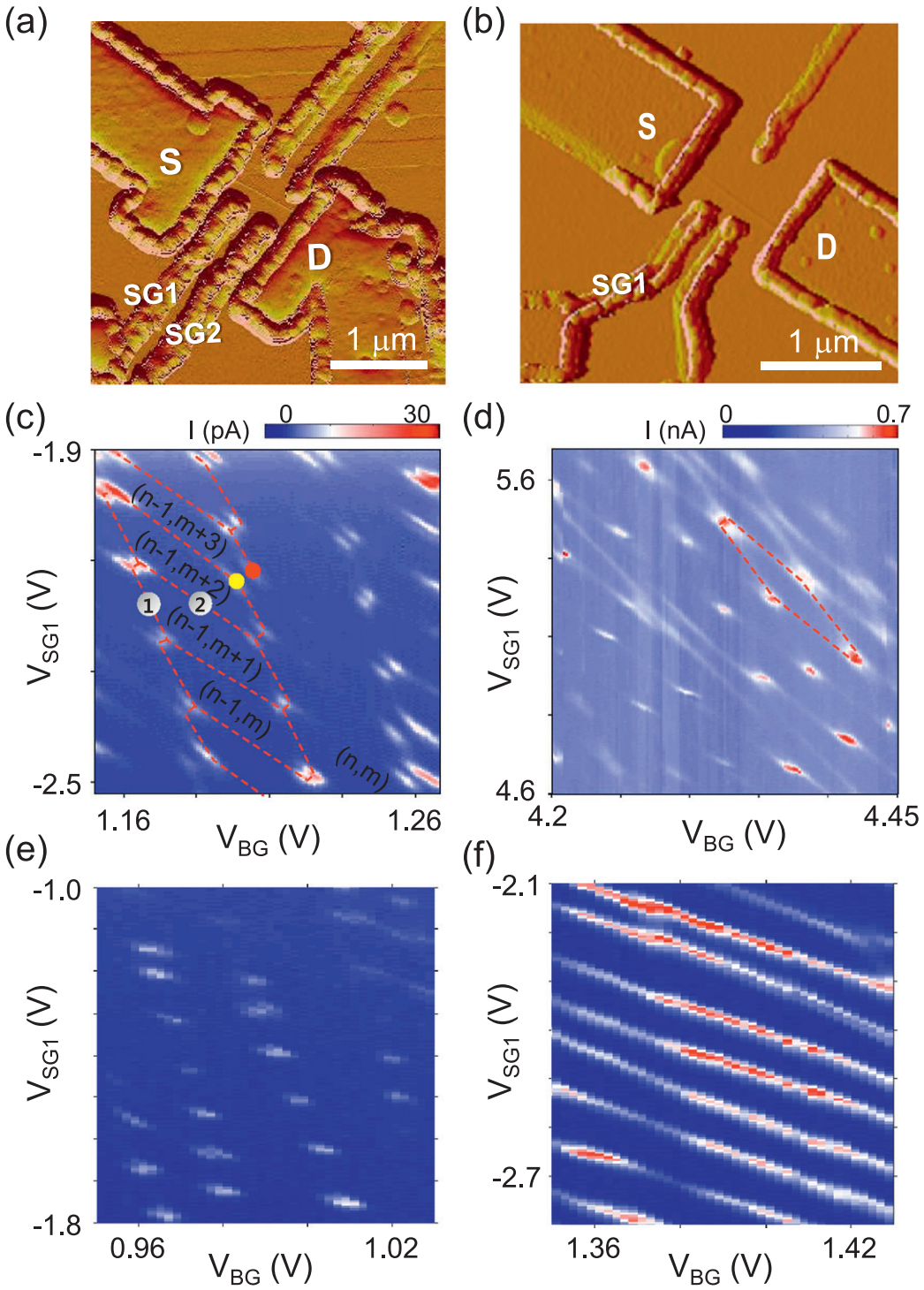

Figure 2. (a), (b) AFM images of CNT field-effect devices, S1 (length $L = 680$ nm, diameter $D \sim 2$ nm) and S2 ($L = 860$, $D \sim 1$ nm) on a 600 nm-thick SiO_2 layer. Here, S, D, SG1 and SG2 represent the source, drain, and side gates 1 and 2, respectively. (c), (d) Charge-stability diagrams for devices S1 and S2 with a gate voltage of $V_{SD} = 50\,\mu$V for varying SG1 and the back gate. The assigned electron numbers (n,m) in QD1 and QD2, respectively, are indicated for each hexagonal region in (c). The hexagonal lines labelled '1' and '2' in (c) represent charging lines for QD1 and QD2, respectively. (e), (f) Charge-stability diagrams for (e) weak and (f) strong coupling regimes, depending on the V_{SG1} and V_{BG} conditions, for device S1.

tunnelling barriers to create multiple QDs in a sub-μm CNT channel by using robust Al_2O_x at the CNT-lead contacts as tunnelling barriers instead of naturally forming Schottky barriers [14], which are sensitive to the electric fields induced by gates near the contacts, resulting in uncontrollable changes in the charge-carrier tunnelling rates. In our device, when a back-gate voltage is applied, the Al_2O_x layers located between the leads and the CNT provide stable tunnelling barriers to form a global potential well along the entire CNT channel.

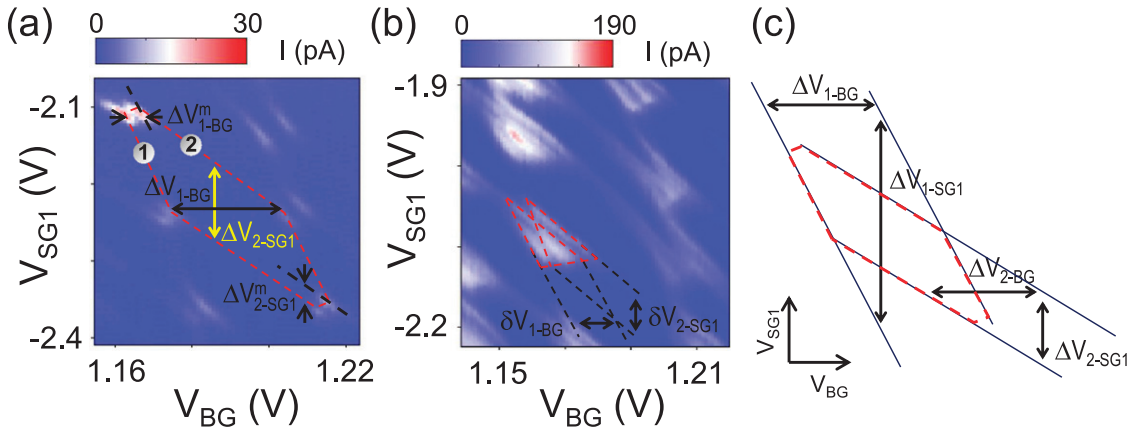

Figure 3. (a) Honeycomb cell structure in a linear transport regime, $V_{SD} = 50\,\mu$V. (b) Triangular structures in a nonlinear transport regime, $V_{SD} = 5$ mV. (c) Schematic diagrams for the estimation of gate capacitances based on the voltage intervals between parallel charging lines.

3. Results and discussion

3.1. Double quantum dots

First, we experimentally obtained charge-stability diagrams (current maps as a function of V_{SG1} and V_{BG} for $V_{SD} = 50\,\mu$V) for the two samples S1 and S2, which are presented in figures 2(c) and (d), respectively. These clearly exhibit honeycomb structures, as denoted by dashed lines on the charging lines. These results indicate that these gate conditions produce an intermediately coupled double-QD structure [4]. By applying various gate conditions to S1, it is also possible to observe weak and strong coupling regimes, as illustrated in figures 2(e) and (f), respectively [2]. For further analysis of the intermediate coupling regime, we focus on the results obtained from S1. The nominal number of electrons in each QD (the number in QD1 and the number in QD2) is indicated in figure 2(c). The yellow (red) point is an electron (hole) triple point, where the electrochemical potentials in the two QDs and the Fermi levels in the leads are aligned. We note that the side gating is more effective at tuning the energy levels of the QDs than at controlling the coupling strength. Based on the dimensions of the honeycomb cell presented in figure 3(a) and the triangular maps in the nonlinear transport region corresponding to $V_{SD} = 5$ mV, presented in figure 3(b), we can obtain the double-QD capacitances depicted in figure 1(a) through the use of certain relations, as discussed below [4]. Here, we note that the back-gate field is coupled to both QDs with nearly the same coupling strength; for instance, ΔV_{1-BG} for QD1 is similar to ΔV_{2-BG} for QD2 in figures 3(a) and (c). By means of the relation $\Delta V_{BG} = |e|/C_{BG}$, we find that $C_{1-BG} = 5.56$ aF and $C_{2-BG} = 6.4$ aF. On the other hand, ΔV_{2-SG1} is smaller than ΔV_{1-SG1} by more than a factor of three; thus, ΔV_{2-SG1} is related to the capacitance of QD2 because the size of QD2 is larger than that of QD1 (see also figures 1(b) and 2(a)). We find that $C_{1-SG1} = 0.5$ aF and $C_{2-SG1} = 1.65$ aF. We also obtain the coupling capacitance between the two QDs as follows: using the relations $(C_{1-BG}/C_1)\delta V_{1-BG} = (C_{2-SG1}/C_2)\delta V_{2-SG1} = V_{SD}$, $\Delta V^m_{1-BG} = \Delta V_{1-BG} C_{12}/C_2$ and $\Delta V^m_{2-SG1} = \Delta V_{2-SG1} C_{12}/C_1$ as well as the capacitances of the leads, $C_S \sim 7.12$ aF and $C_D \sim 5.32$ aF, we find that $C_{12} \sim 2.39$ aF. We note that the total capacitance for a QD should take the following form: $C_{1(2)} = C_{S(D)} + C_{1-BG(2-SG1)} + C_{1-SG1(2-BG)} + C_{12}$, where the third term in the relation is interpreted as a so-called 'cross-talk' effect. The capacitance values obtained above are also taken into consideration for the triple-QD calculations presented below.

3.2. Triple quantum dots

Next, we turned on the second local side gate SG2 in addition to SG1 to produce the triple QDs described in figure 1(c). Figure 4(a) presents a charge-stability diagram for device S1 with varying SG1 and SG2 voltages of $V_{BG} = 1.23$ V and $V_{SD} = 0.6$ mV. In the upper region with respect to the black dashed line, single-dot behaviour is evident where the inter-dot coupling is sufficiently strong, although wiggle structures are apparent on the charging lines. This behaviour changes when the gate conditions lie in the opposite region, where the charging-line intensity is diminished, producing a complicated pattern. The magnified configuration pictured in figure 4(b) exhibits a rather different structure than that of the double-QD case represented in figures 2(c) and (d). For instance, the diagram essentially consists of three charging lines (the dashed black, red and white lines) with different slopes, which indicate the presence of three QDs in the CNT. We can also identify two distinct electron-hole triple-point pairs, indicated by the dashed green and red circles. The pair indicated in green exhibits a weaker inter-dot coupling than the pair indicated in red because the coupling strength is inversely proportional to the distance between the electron-hole triple points. Importantly, we frequently observe slightly curved charging-line pairs, as representatively indicated by the dashed black circle, which represents another electron-hole triple-point pair. For geometrical reasons, it is expected that the inter-dot coupling between QD1 and QD3 will be the weakest among the three possible combinations for two-QD coupling in three QDs (see figures 1(c) and 2(a)); therefore, the pair indicated in green should be associated with the charge transfer between QD1 and QD3. In addition, ΔV_3 is smaller than ΔV_1 in figure 4(b); the QD that corresponds to the dashed white charging lines is more strongly coupled to

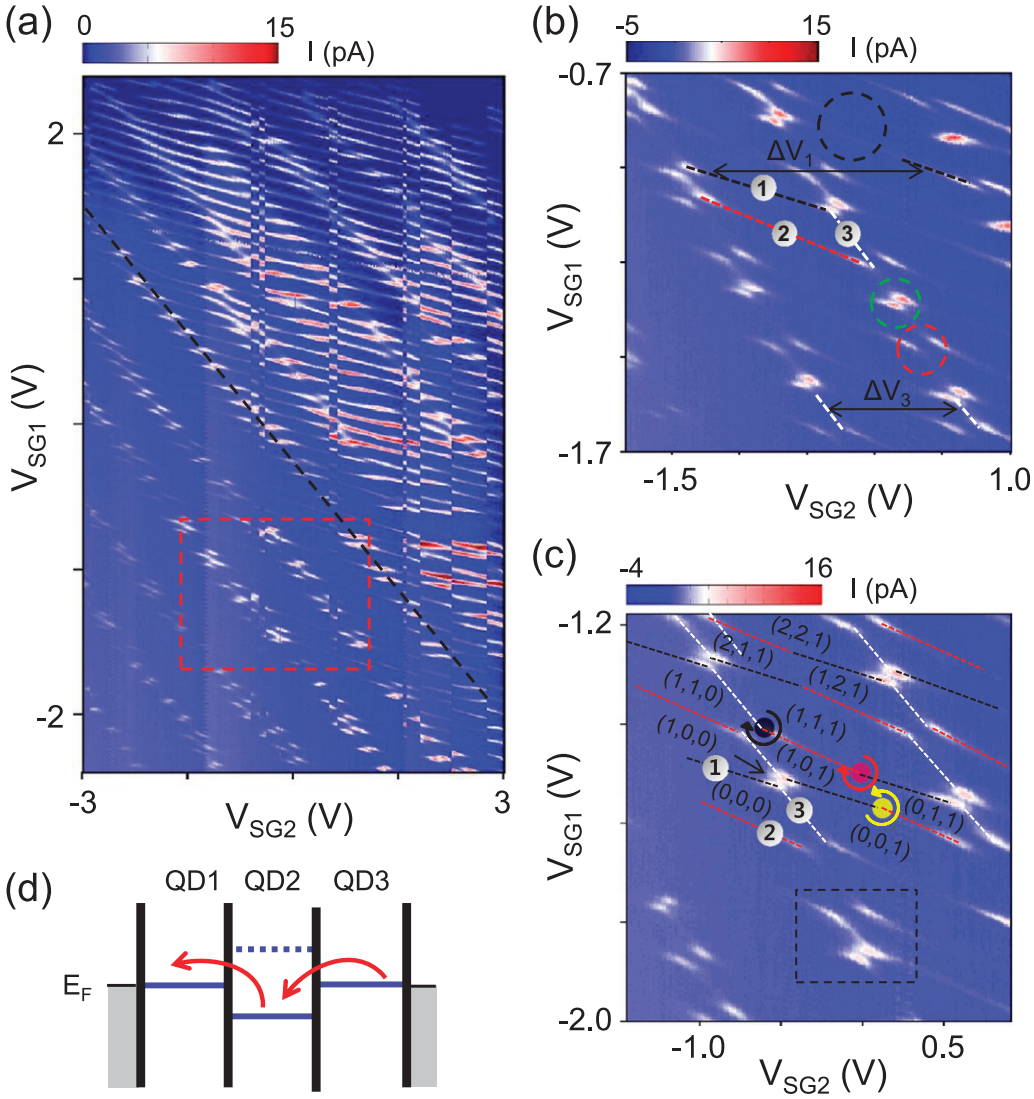

Figure 4. (a) Charge-stability diagram for varying SG1 and SG2 voltages at $V_{BG} = 1.23$ V and $V_{SD} = 0.6$ mV. (b) Triple-QD structure in the dashed-box region in (a). Dashed circles indicate electron-hole triple points. (c) Nominal number of electrons for each ground state in the triple QD. The dashed box indicates a candidate region for the observation of a hole quadruple point. (d) Energy diagram for the second-order co-tunneling process between QD1 and QD3 that corresponds to the anti-crossing charging lines indicated by an arrow in (c).

V_{SG2} than is the QD that corresponds to the black lines. Thus, we conclude that the white and black dashed lines are associated with QD3 and QD1, respectively. Naturally, the remaining red dashed charging line corresponds to QD2. Thus, the labels '1', '2' and '3' that accompany the three different charging lines correspond to QD1, QD2 and QD3, respectively, in figure 4(b).

Based on the above analysis, we assign nominal charge numbers to a selected diagram in figure 4(c): (n,m,l), where n, m and l are the numbers of electrons in QD1, QD2 and QD3, respectively. More specifically, we assign the charge numbers as follows: whenever charging lines cross, the charge numbers of the corresponding QDs are increased by one; for instance, the crossings of the black, red and white dashed lines in figure 4(c) each increase the charge numbers of QD1, QD2 and QD3 by one, respectively. As expected, the two nearest triple points (anti-crossing charging lines denoted by an arrow) correspond to the charge transfer between QD1 and QD3, which has the weakest coupling strength. We believe that this transfer occurs via a second-order co-tunnelling process that bypasses the Coulomb-blockaded QD2 (see figure 4(d)), resulting in a molecular coupling state even though there is no direct tunnelling coupling between QD1 and QD3 [11].

Such a configuration, in which molecular coupling states exist between all possible two-QD combinations in a triple QD system, has previously been achieved in a triangular QD design in GaAs/InGaAs 2DEG systems [22–24]. Specifically, direct coherent coupling between the outer QDs in a linear triple-QD system created in a 2DEG system has been observed by means of a bipolar spin blockade [12] and a charge-detection technique [13]. In a previously reported study regarding a serially connected triple-QD system formed in a CNT [11], however, QD1 and QD3 only operated independently because of relatively weak inter-dot couplings. In our case, sufficiently high inter-dot coupling strengths were

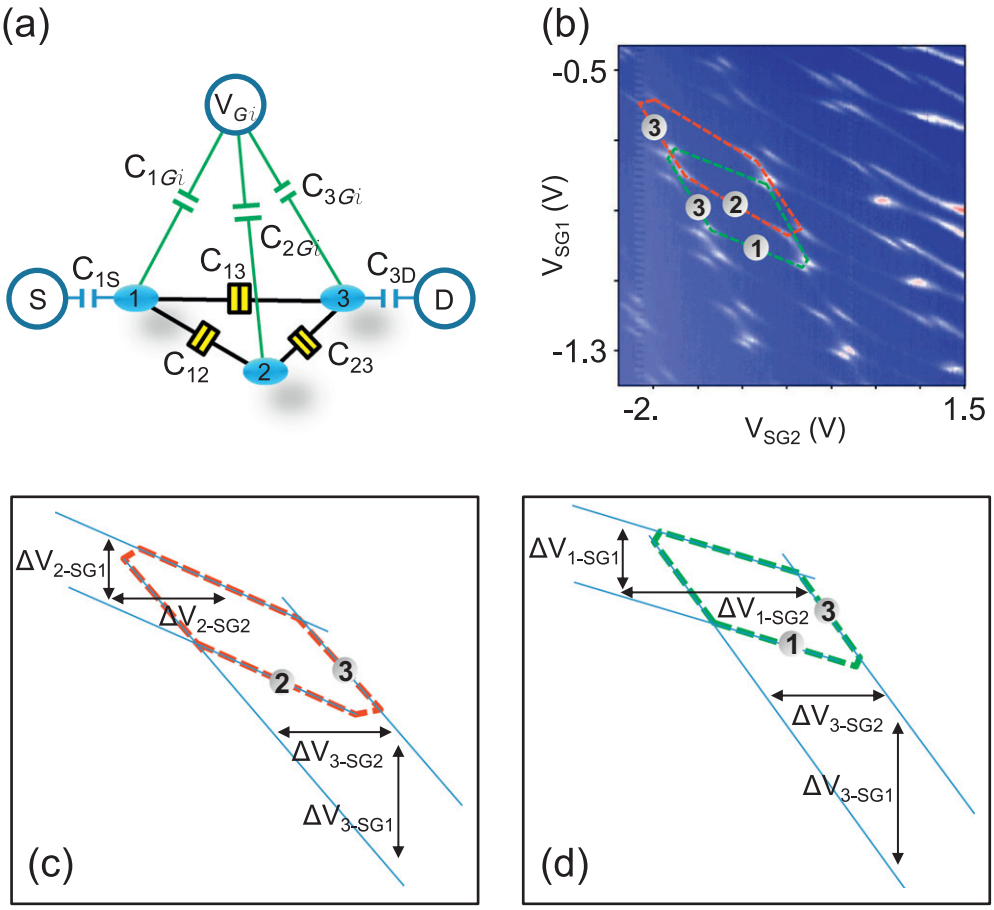

Figure 5. (a) Schematic diagram of the capacitive interaction model for a triple-QD system. (b) Re-plot of figure 4(b) for the estimation of gate capacitances based on the voltage intervals between parallel charging lines in (c) and (d).

observed to lead to electron-hole triple points between the outer dots. Interestingly, if two separate hole triple points, as indicated respectively by the black and red dots for QD2-QD3 and QD1-QD2 (see the black and red circular arrows), satisfy the proper gate conditions, a hole quadruple point will arise for QD1-QD2-QD3. In this case, the three electrochemical potentials in the three QDs are aligned with the Fermi levels in the two leads.

3.3. Capacitive interaction model

To confirm our findings, we simulated the charge-stability diagram of a triple-QD system based on a capacitive interaction model, following References [11, 24, 25]. Figure 5(a) depicts a schematic of a circuit model with three QDs. Although our three QDs are serially distributed along the CNT, we consider all possible inter-dot couplings between the three dots, indicated by C_{12}, C_{23} and C_{13}, to account for the coupling between QD1 and QD3. C_{1S} and C_{3D} are the QD1-source and QD3-drain capacitances, respectively. The electrostatic energy of the triple-QD system is expressed as follows:

$$E(n_1, n_2, n_3) = \sum_{i=1,2,3} U_i Q_i^2 + \sum_{i \neq j} U_{ij} Q_i Q_j, \qquad (1)$$

where U_i is the intradot capacitance energy of the ith QD, U_{ij} is the electrostatic inter-dot coupling energy between QDs i and j, $Q_i = n_i - \sum_j c_{ij} V_{Gj}$ is the effective charge, n_i is the excess charge, $\sum_j c_{ij} V_{Gj}$ is the gate charge of QD i, V_{Gi} represents the electrostatic potential of the gate, and the c_{ij} are coupling coefficients (V_{G1}, V_{G2} and V_{G3} for SG1, SG2 and the back gate, respectively). The single-particle-level spacing and the Zeeman energy are ignored in this formulation. In figure 4(b), because the distance between the triple points that correspond to the same two-QD group changes only slightly as a function of the gate voltages, the inter-dot coupling strength for the QDs is not sensitive to the changing side-gate voltages under investigation. In our model of the examined region, we therefore neglect the effect of the side gates on the inter-dot coupling energy.

To calculate the electrostatic energy of each QD based on equation (1), using the relation $\Delta V_G = |e|/C_G$, we first determine the site-gate capacitance for each QD based on the voltage spacing of the hexagons depicted in figures 5(b)–(d): $\Delta V_{3-SG2} = 1.065$ V ($C_{3G2} = 0.151$ aF), $\Delta V_{2-SG1} = 0.178$ V ($C_{2G1} = 0.9$ aF), $\Delta V_{3-SG1} = 0.453$ V ($C_{3G1} = 0.353$ aF), $\Delta V_{2-SG2} = 1.25$ V ($C_{2G2} = 0.128$ aF), $\Delta V_{1-SG1} = 0.195$ V ($C_{1G1} = 0.8215$ aF) and $\Delta V_{1-SG2} = 1.859$ V ($C_{1G2} = 0.086$ aF). For the capacitances between the back gate and the QDs, we consider values similar to those for the double-QD case. For the inter-dot capacitances, we use $C_{12} = 2.39$ aF, $C_{23} = 2.1$ aF

and $C_{13} = 0.6$ aF. Here, the C_{12} value obtained from the double-QD system is adopted under the assumption that C_{12} does not significantly differ between the two cases. The other inter-dot capacitance values were determined based on which values yielded the best simulation results with respect to the distance between the electron and hole triple points.

Then, the total capacitance of each QD is obtained as follows: $C_1 = 13.27$ aF, $C_2 = 8.41$ aF and $C_3 = 10.82$ aF, where $C_1 = C_{1G1} + C_{1G2} + C_{1G3} + C_{12} + C_{13} + C_{1S}$, $C_2 = C_{2G1} + C_{2G2} + C_{2G3} + C_{12} + C_{23}$, $C_3 = C_{3G1} + C_{3G2} + C_{3G3} + C_{13} + C_{23} + C_{3D}$, $C_{1S} = 7.12$ aF, and $C_{3D} = 5.32$ aF. Here, we used the source and drain capacitances obtained from the double-QD analysis. In summary, all capacitances between QD i ($i = 1, 2, 3$) and V_{Gj} ($j = 1, 2, 3$), C_{iGj} in equation (1) can be expressed as follows:

$$\begin{pmatrix} C_{1G1} & C_{1G2} & C_{1G3} \\ C_{2G1} & C_{2G2} & C_{2G3} \\ C_{3G1} & C_{3G2} & C_{3G3} \end{pmatrix} = \begin{pmatrix} 0.8215 & 0.086 & 5.7 \\ 0.9 & 0.128 & 6 \\ 0.353 & 0.151 & 5.8 \end{pmatrix}, \text{ in the aF unit.} \quad (2)$$

The charging energies of each QD i are [26] $U_1 = K \times \left(C_2 C_3 - C_{23}^2\right) = 12.8$ meV, $U_2 = K \times \left(C_1 C_3 - C_{13}^2\right) = 21.2$ meV and $U_3 = K \times \left(C_2 C_1 - C_{12}^2\right) = 15.7$ meV. The electrostatic coupling energies between QD i and QD j are $U_{12} = K \times \left(C_3 C_{12} + C_{13} C_{23}\right) = 4$ meV, $U_{23} = K \times \left(C_1 C_{23} + C_{12} C_{13}\right) = 4.3$ meV and $U_{13} = K \times \left(C_2 C_{13} + C_{23} C_{12}\right) = 1.5$ meV, where the coefficient is defined as $K = \frac{e^2}{C_1 C_2 C_3 - 2C_{12} C_{13} C_{23} - \left(C_3 C_{12}^2 - C_2 C_{13}^2 - C_1 C_{23}^2\right)}$.

Figure 6 presents a stability diagram calculated for $V_{BG} = 1.18$ V. Here, the numbers of electrons (n,m,l) were determined by searching for a ground state of the system based on the electrostatic energy of each QD while varying the gate voltages. Although the value of V_{BG} calculated in this manner deviates slightly from the experimental value, the results are nearly consistent with the experimental data presented in figure 4(c). For instance, the results indicate three different types of charging lines, denoted by '1', '2' and '3'. We can also identify the red and yellow solid circles on the curved charging lines in figure 4(c) as hole and electron triple points, respectively, for QD1-QD2 (see the red and blue circular arrows in figure 6). On the other hand, the black dots correspond to hole triple points for QD2–QD3 (see the black circular arrow). The stability diagram indicates two possible tunnelling sequences for an electron passing from QD1 to QD3 through QD2: (n,m,l) → (n − 1,m + 1,l) → (n − 1,m,l + 1) and (n,m,l) → (n,m − 1,l + 1) → (n − 1,m,l + 1), e.g., (9,8,10) → (8,9,10) → (8,8,11) and (8,8,9) → (8,7,10) → (7,8,10), respectively. Importantly, in addition to sequential tunnelling, direct tunnelling processes between QD1 and QD3 with anti-crossing charging lines are

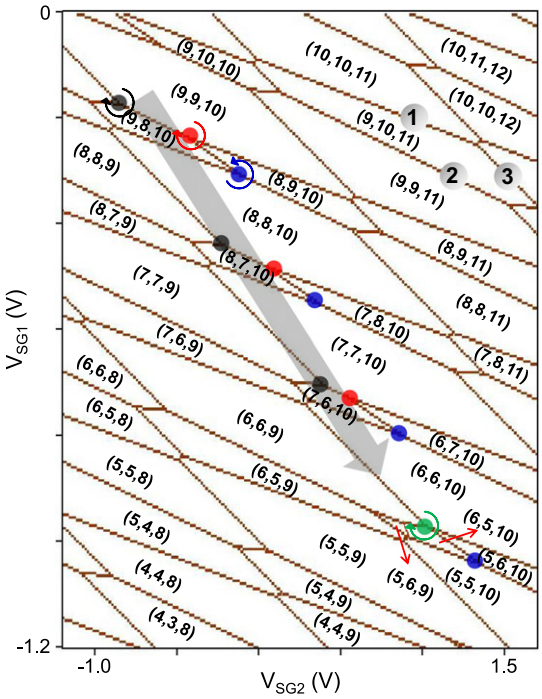

Figure 6. Calculated stability diagram. The red and blue dots indicate hole and electron triple points, respectively, for the QD1–QD2 coupling. The black dots correspond to hole triple points for the QD2–QD3 coupling. When the black and red dots converge under proper gate conditions, a hole quadruple point is formed, as indicated by the green dot.

evident, e.g., (8,7,9) → (7,7,10), as observed in the experiments. Note that the black and red dots approach each other when the two side-gate conditions change along the QD3 charging line (or when the electrochemical potentials for each QD are rearranged), as indicated by the grey arrow. At $V_{SG1} \sim -0.95$ V and $V_{SG2} \sim 1.1$ V, the two hole triple points nearly overlap, and a hole quadruple point appears, as indicated by the green solid circle. In this case, a hole can be transported as follows: 'Source' → 'QD1' → 'QD2' → 'QD3', i.e., (6,6,10) → (5,6,10) → (6,5,10) → (6,6,9), following the green circular arrow. This behaviour is consistent with previous experimental observations of the quadruple point in a triple-QD system formed in a GaAs/AlGaAs 2D gas system [22, 23, 25]. In our experiments, the hole triple points depicted in black and red in figure 4(c) might correspond to those of the (8,7,10) state depicted in figure 6. If this is the case, the dashed-box region in figure 4(c), which exhibits a nearly straight charging line, may be a region in which the hole quadruple point can be observed, although the data are not conclusive. To observe such a quadruple point in experiments, charge-sensitive or phase-sensitive measurement schemes would be needed [22, 26].

4. Conclusion

In this paper, we demonstrated multiple-QD formation in CNTs using local side and global back gates. To prevent problems arising due to the modulation of the Schottky

barriers between the CNT and the metal contacts near gate fields, we introduced an artificial Al_2O_x tunnelling barrier at the contacts. We successfully produced single, double and triple QDs using the local side gates, while the back gate formed a global potential well between the two contacts of the CNT. Notably, we observed the formation of a distant molecular coupling state between QD1 and QD3 through the Coulomb-blockaded QD2, possibly via a second-order co-tunnelling process, when the inter-dot coupling strengths were sufficiently high in a linear triple-QD system formed in a CNT. This finding was also supported by calculations based on a capacitive interaction model. Our design for multiple QDs based on local side gates could provide a feasible method of constructing an integrated QD system for future quantum-engineering applications.

Acknowledgments

We thank Prof. H-S Sim for fruitful discussion. We also thank Dr. Eun-Kyoung Jeon for the illustration in figure 1(a). This work was supported by the Korea Research Institute of Standards and Science under the project 'Convergent Science and Technology for Measurements at the Nanoscale', grant 14011018 and the National Research Foundation of Korea (NRF) (nos. 2011-0015895, 2012-R1A2A1A-03010558 and NRF-2012-M3C1A1-048861).

References

[1] Park H, Park J, Lim A K L, Anderson E H, Alivisatos A P and McEuen P L 2000 *Nature* **407** 57
[2] Mason N, Biercuk M J and Marcus C M 2004 *Science* **303** 655
[3] Schroer M D, Petersson K D, Jung M and Petta J R 2011 *Phys. Rev. Lett.* **107** 176811
[4] van der Wiel W G, Franceschi S D, Elzerman J M, Fujisawa T, Tarucha S and Kouwenhoven L P 2002 *Rev. Mod. Phys.* **75** 1
[5] Paaske J, Rosch A, Wölfle P, Mason N, Marcus C M and Nygård J 2006 *Nat. Phys.* **2** 460
[6] Kim J, Kim J-R, Lee J-O, Park J W, So H M, Kim N, Kang K, Yoo K-H and Kim J-J 2003 *Phys. Rev. Lett.* **90** 166403
[7] Liang W, Bockrath M, Bozovic D, Hafner J H, Tinkham M and Park H 2001 *Nature* **411** 665
[8] Kim B-K, Ahn Y-H, Kim J-J, Choi M-S, Bae M-H, Kang K, Lim J S, López R and Kim N 2013 *Phys. Rev. Lett.* **110** 076803
[9] Biercuk M J, Garaj S, Mason N, Chow J M and Marcus C M 2005 *Nano Lett.* **5** 1267
[10] Laird E A, Pei F and Kouwenhoven L P 2013 *Nat. Nanotechnol.* **8** 565
[11] Grove-Rasmussen K, Jørgensen H I, Hayashi T, Lindelof P E and Fujisawa T 2008 *Nano Lett.* **8** 1055
[12] Busl M *et al* 2013 *Nat. Nanotechnol.* **8** 261
[13] Braakman F R, Barthelemy P, Reichl C, Wegscheider W and Vandersypen L M K 2013 *Nat. Nanotechnol.* **8** 432
[14] Steele G A, Gotz G and Kouwenhoven L P 2009 *Nat. Nanotechnol.* **4** 363
[15] Jung M, Schindele J, Nau S, Weiss M, Baumgartner A and Schönenberger C 2013 *Nano Lett.* **13** 4522
[16] Javey A, Kim H, Brink M, Wang Q, Ural A, Guo J, McIntyre P, McEuen P, Lundstrom M and Dai H 2002 *Nat. Mater.* **1** 241
[17] Li S, Yu Z and Burke P J 2004 *J. Vac. Sci. Technol.* B **22** 3112
[18] Chen Y-F, Dirks T, Al-Zoubi G, Birge N O and Mason N 2009 *Phys. Rev. Lett.* **102** 036804
[19] Biercuk M J, Mason N, Martin J, Yacoby A and Marcus C M 2005 *Phys. Rev. Lett.* **94** 026801
[20] Sapmaz S, Meyer C, Beliczynski P, Jarillo-Herrero P and Kouwenhoven L P 2006 *Nano Lett.* **6** 1350
[21] Gotz G, Steele G A, Vos W-J and Kouwenhoven L P 2008 *Nano Lett.* **8** 4039
[22] Gaudreau L, Studenikin S A, Sachrajda A S, Zawadzki P, Kam A, Lapointe J, Korkusinski M and Hawrylak P 2006 *Phys. Rev. Lett.* **97** 036807
[23] Rogge M C and Haug R J 2009 *New J. Phys.* **11** 113037
[24] Seo M, Choi H K, Lee S-Y, Kim N, Chung Y, Sim H-S, Umansky V and Mahalu D 2013 *Phys. Rev. Lett.* **110** 046803
[25] Schröer D, Greentree A D, Gaudreau L, Eberl K, Hollenberg L C L, Kotthaus J P and Ludwig S 2007 *Phys. Rev.* B **76** 075306
[26] Schroer M D, Jung M, Petersson K D and Petta J R 2012 *Phys. Rev. Lett.* **109** 166804